Three-pion production on complex nuclei at 23 GeV/c

T. J. Roberts* and U. E. Kruse
University of Illinois at Urbana-Champaign, Illinois 61801

R. E. Edelstein, E. J. Makuchowski, C. M. Meltzer,† E. L. Miller,‡ and J. S. Russ
Carnegie-Mellon University, Pittsburgh, Pennsylvania 15213

B. Gobbi, J. L. Rosen, and H. A. Scott
Northwestern University, Evanston, Illinois 60201

S. L. Shapiro¶ and L. Strawczynski
University of Rochester, Rochester, New York 14627
(Received 1 February 1977)

The production of three pions has been examined in interactions of 23-GeV/c π^- with complex nuclei. A partial-wave analysis of the three-pion system has been performed showing that the spin-parity structure is very similar to the one produced in hydrogen. The production cross section for various nuclei have been compared with an optical-model calculation. In the A_1 region the absorption cross sections obtained from the model are 25 mb for $J^P = 1^+$ and 60 mb for $J^P = 0^-$.

This paper describes an analysis of an experiment measuring three-pion production at 23 GeV/c with various complex nuclei as targets. These reactions are of the form

$$\pi^- A \to \pi^+\pi^-\pi^- A ,$$

where A is one of the nuclear targets: carbon, aluminum, copper, silver, or lead. We present results which are more comprehensive than those in our preliminary Letter[1] and include an optical-model analysis of them. In the interest of brevity, only the briefest possible mention will be made of either the experimental apparatus[2] or of the Illinois method of partial-wave analysis,[3] which was adapted essentially intact from previous analyses.

Ever since Glauber's classic papers on high-energy interactions with nuclei,[4] experimentalists have been using these and similar "optical" models in the analysis of interactions with nuclei, with generally good success. Glauber's original analysis of elastic scattering is especially notable since it exhibits excellent agreement between the optical model and experiment.

In recent years, theoretical interest in interactions within nuclei has engendered a growing body of literature on the subject, much of which casts doubts upon the basic ideas of these optical models (usually by pointing out that these models ignore "inelastic screening"[5] or some related phenomenon). Experimentally, nonelastic reactions in nuclei have also been explored, and reasonable agreement has been found between the model and the experimental results. This holds true for this present analysis. There are, however, some systematic differences as explained below in Sec. V, leaving open the invitation for improvements in both the experimental techniques and the theoretical interpretations.

Two terms dealing with nuclear production processes will appear throughout this report: coherent and incoherent production. These terms come from optical models for nuclear processes, since these models build the cross section from two parts. In one part, the production amplitudes on the individual nucleons are summed, then squared, to yield the coherent production cross-section; this is obtained when the nucleus remains in its ground state. The other part is a sum of intensities for production on the individual nucleons, thus giving the incoherent cross section, and is obtained when the nucleus is excited or breaks up. The coherent production depends upon the properties of the entire nucleus (such as shape), dominates at low momentum transfer, and exhibits maxima and minima similar to Fraunhofer diffraction from a gray sphere. The incoherent production exhibits properties of the production from single nucleons, and dominates at moderate-to-large momentum transfers. This is illustrated in Fig. 1, which shows both model calculations and the experimental data, for silver.

This paper is divided into five sections: Section I contains an abbreviated description of the apparatus; Sec. II introduces the partial-wave analysis; Sec. III describes our experimental and partial-wave results; Sec. IV provides a description of our optical model for three-pion production, and Sec. V presents the results of our optical-model analysis of these data. Finally,

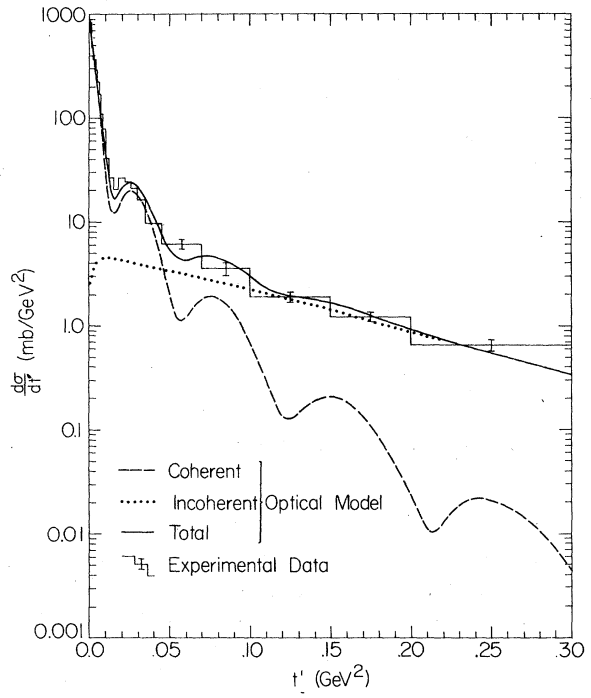

FIG. 1. The coherent, incoherent, and total optical-model calculations for silver, along with the experimental data, $1.0 < M_{3\pi} < 1.2$ GeV.

Sec. VI will attempt briefly to summarize these results and conclusions.

I. RESUMÉ OF THE APPARATUS

These data were acquired at the Brookhaven National Laboratory using the Lindenbaum-Ozaki Mark-I Spectrometer[2] with a beam of 22.58-GeV/c pions. The nuclear targets were approximately 0.1 radiation lengths long, and were surrounded by γ-sensitive veto counters (with holes front and rear for the fast particles). These veto counters were intended to veto events with slow π^0's, and events in which the nucleus made either a fast γ-ray transition, or broke up with some charged fragment energetic enough to leave the target. The trigger basically required: (1) a good beam track (identified as a pion), (2) the absence of any veto counter, and (3) at least two charged particles in front of and behind the analyzing magnet.

There are two classes of data considered, called "1C" and "0C" events. 1C events have three reconstructed tracks which traverse the analyzing magnet, so the momentum and direction of all three pions is measured, and there is a one-constraint kinematic fit available. 0C events have two complete tracks, and one which does not traverse the magnet (so only its direction is measured); these events have no extra constraint for a kinematic fit. In all results presented here we have combined these two classes of events into one sample, in order to reduce statistical errors. For the carbon target, we have analyzed the 1C sample separately, and have obtained answers consistent with those from the combined sample. 1C events comprise approximately 35% of the combined data sample, as indicated in Table I.

II. PARTIAL-WAVE ANALYSIS

The Illinois method of partial-wave analysis has been copiously described[3]; we have used the same method as for hydrogen targets, with only slight modification. We assume that the target affects only the production of the "3π system," but does not affect its decay into three pions (see Sec. III D). Thus, only the $M_{3\pi}$ and t' dependence of the density matrix is affected by the nucleus. We approximate the t' dependence with a sum of two exponentials[1] fitted to the (efficiency-corrected) data (these approximate the coherent and incoherent contributions of Sec. IV). The $M_{3\pi}$ dependence is not altered, because it is only the variation over a given bin which is important, and that is essentially unchanged from hydrogen.

In this analysis, the 3π system is considered to be a definite object (mass = $M_{3\pi}$, spin-parity = J^P) produced at a point within the nucleus, which decays into a "bachelor" pion and a dipion system. The dipion then decays into two pions, resulting in the three-pion final state which is observed. States are named by the quantum numbers

TABLE I. Amount of data taken.

Element	3-prong reconstr.	0C events	1C events	0C and 1C events	Normalization (μb/event)
carbon	83 675	34 312	19 528	53 840	0.0395
aluminum	48 163	18 491	11 474	29 965	0.135
copper	38 303	13 137	8285	21 422	0.294
silver	31 492	10 445	6476	16 921	0.497
lead	19 936	5728	3479	9207	1.019

$J^P(LS)M^\eta$: J^P is the spin-parity of the 3π system, S is the spin of the dipion system, L is the relative angular momentum of the dipion and the bachelor pion, M is the magnitude of the Z projection (in t-channel helicity axes) of J, and $(-\eta)$ is the eigenvalue for reflections in the production plane (here $0 \leq M \leq J$, $\eta = \pm 1$, instead of the usual $-J \leq M \leq J$).

In our density-matrix approach, the cross section is written $[a, b \equiv J^P(LS)M^\eta]$

$$W(s,t,M_{3\pi},\vec{\mathrm{x}}) = \sum_{ab} \mathfrak{M}_a(\vec{\mathrm{x}})\, \tilde{\rho}_{ab}(s,t,M_{3\pi})\, \mathfrak{M}_b^*(\vec{\mathrm{x}}), \tag{2.1}$$

$$\mathfrak{M}_{J^P(LS)M^\eta} = \sum_{m\mu} \langle JM | LSm\mu \rangle (P_1)^L Y_L^m(\theta_1,\phi_1) \times \frac{1}{m_s^2 - s_1 - i m_s \gamma_s(s_1)} \times (\bar{P}_1)^s Y_s^\mu(\bar{\theta}_1,\bar{\phi}_1) + (1-2), \tag{2.2}$$

where s = total center-of-mass energy squared, $-t$ = four-momentum transfer squared, $M_{3\pi}$ = three-pion mass, and $\vec{\mathrm{x}}$ indicates the variables describing the decay (only five of which are independent): θ_1, ϕ_1, P_1 describe $(\pi^+\pi_2^-)$ in 3π rest frame, $\bar{\theta}_1$, $\bar{\phi}_1$, $\bar{P}_1$ describe π^+ in $(\pi^+\pi_2^-)$ rest frame, s_1 is the $(\pi^+\pi_2^-)$ mass squared,

$$\gamma_s(s_1) = \Gamma_s \frac{m_s}{\sqrt{s_1}} \left(\frac{P_1}{P_0}\right)^{2s+1}, \tag{2.3}$$

m_s, Γ_s describe the dipion propagator for the resonance of spin s.

The relation between the conventional $-J \leq M \leq J$ states above and our usual $M\eta$ states is

$$\mathfrak{M}_{J^P(LS)M^\eta} = \lambda_M [\mathfrak{M}_{J^P(LS)M} + \eta(-1)^{J+M+1} \mathfrak{M}_{J^P(LS)-M}], \tag{2.4}$$

with $\lambda_M = \frac{1}{2}$ if $M = 0$, $\lambda_M = 1/\sqrt{2}$ if $M \neq 0$. The density matrix describing the production is

$$\tilde{\rho}_{ab} = f_a(M_{3\pi},t)\, \rho_{ab} f_b^*(M_{3\pi},t), \tag{2.5}$$

$$f_{J^P(LS)M^\eta}(M_{3\pi},t') = (\sqrt{t'})^M (\mathrm{Be}^{-\beta t'} + \mathrm{Ce}^{-\gamma t'}). \tag{2.6}$$

The f's are the double-exponential fits to the data, as in Ref. 1.

The parameters in the fit are the ρ_{ab}'s, which are subject to the constraint that ρ be positive-definite. We make the usual reduction by assuming maximal interference ("coherence") between states of the same J^P but of a different LS. These ρ_{ab}'s are determined from the data in the usual maximum-likelihood manner, and, as the normalization includes the experimental detection efficiency, the results are corrected for the acceptance of our apparatus.

The states included in this analysis are listed in Table II. We have tried all states with $J \leq 3$, $L \leq 2$, and appropriate values of M—those listed are the only ones found to be "important" (i.e., more than 1 standard deviation away from zero.) "Flat" is isotropic in all decay variables, and is intended to account for backgrounds not included in the above sequential decay scheme. In all of our fits the amount of "Flat" is statistically consistent with zero.

TABLE II. States included in partial-wave analysis.

$0.8 < M_{3\pi} < 1.2$ GeV	$1.2 < M_{3\pi} < 2.0$ GeV
Flat	Flat
$0^-(S \to \epsilon\pi)0^+$	$0^-(S \to \epsilon\pi)0^+$
$0^-(P \to \rho\pi)0^+$	$0^-(P \to \rho\pi)0^+$
$1^+(S \to \rho\pi)0^+$	$1^+(S \to \rho\pi)0^+$
$1^+(P \to \epsilon\pi)0^+$	$1^+(P \to \epsilon\pi)0^+$
$2^-(P \to \rho\pi)0^+$	$2^-(S \to f\pi)0^+$
$2^+(D \to \rho\pi)1^+$	$2^-(P \to \rho\pi)0^+$
	$2^+(D \to \rho\pi)1^+$
	$3^+(P \to f\pi)0^+$
	$3^+(D \to \rho\pi)0^+$

III. EXPERIMENTAL AND PARTIAL-WAVE RESULTS

In describing the production of three-pions from nuclei, there are four kinematic variables required to specify that production (plus an uninteresting azimuthal angle which we shall ignore): s, t, $M_{3\pi}$, A. In this experiment the beam momentum is always 22.6 GeV/c, so there is only one value of s for each target element. The production cross sections as a function of the other three variables are, however, very interesting, especially when decomposed into the various spin-parity components. These distributions will form the main part of this section, along with some basic production cross sections, and a few other observations.

While most figures in this section include optical-model curves (see Sec. V below), we have attempted to keep this discussion as model independent as possible. We have used the terms "coherent" and "incoherent" to describe the other two major segments of the production, because we feel that those kinds of phenomena are so general that the terms are not restricted to optical models. The separation between the two types of production can only be performed statistically from the t' distributions. This does require some model for the processes, but in practice the difference between models is negligible. For example, when we fit the data with the very simple phenomenological model of Ref. 1,

$$\frac{d\sigma}{dt} = Be^{-\beta t'} + Ce^{-\gamma t'}, \tag{3.1}$$

we obtain essentially the same cross sections for coherent and incoherent parts as with the fits using the optical model presented in Sec. IV.

A. Cross sections

In this section we present the cross-section information and the coefficient β of t' in the exponential dependence for the coherent region. The results are collected in Table III. The quoted errors take into account both the statistical errors and the systematics from element to element; they do not include an additional 10% error in the overall normalization.

The coherent cross section was obtained by subtracting the incoherent contribution from the total cross section for the indicated t' region. This incoherent subtraction was performed by fitting the incoherent model (for each element, in each $M_{3\pi}$ interval) to the large-t' data, and then calculating the incoherent production within the quoted (low-t') bin. The uncertainties in this procedure are smaller than the element-to-element systematic errors.

B. Structure in three-pion mass

In three-pion production from nuclei, the major effect of the nuclear vertex on the three-pion mass distribution is to suppress the high-$M_{3\pi}$ production relative to the low-$M_{3\pi}$ production. The production amplitude is proportional to the overlap integral of the three-pion wave function and the pion (beam) wave function, integrated over the nuclear density. These wave functions have different wavelengths, due to the momentum transfer $\vec{q}$, and their overlap is smaller for larger nuclei (because the nuclear density is normalized). Since larger $M_{3\pi}$ implies larger $\vec{q}_{min}$ (the minimum kinematically allowed momentum transfer), the amplitude for large $M_{3\pi}$ is smaller than that for small $M_{3\pi}$ (for the same nucleus). This low/high $M_{3\pi}$ ratio also increases with A.

This A-dependent suppression is readily evident in Fig. 2, which shows the low-t' (mainly coherent) three-pion mass distributions for all five target nuclei. Similar distributions for high-t' (mainly incoherent) production, shown in Fig. 3, show no such A-dependent suppression, as the incoming and outgoing wave functions need not overlap over the entire nucleus, but merely over a single nucleon.

The other structure of interest here is the spin-parity composition of the production, as a function of $M_{3\pi}$; the major contributing states are shown in Figs. 4 and 5, illustrating the low-t' and high-t' regions. Clearly present are the A_1 ($1^+S \to \rho\pi$), the A_2 ($2^+D \to \rho\pi$), and the A_3 ($2^-S \to f\pi$), with a fair amount of 0^- and 3^+ background. These features are so similar to the hydrogen data[3] as to require no further comment. The relative phases of a few selected states are shown in Fig. 6; again, all of them follow the hydrogen results quite closely.

C. Structure in momentum transfer

The $M_{3\pi}$ distributions above show only a slight difference between coherent and incoherent pro-

TABLE III. Three-pion production cross sections. Errors include statistical and element-to-element systematic errors only.

$M_{3\pi}$ region (GeV)	Element	t' region (GeV^2)	Coherent 3π cross section (mb)	Total 3π cross section (mb)	t' dependence β (GeV^{-2})
1.0–1.2	C	$0<t'<0.040$	0.854 ± 0.065	0.918 ± 0.065	75.1 ± 1.6
	Al	$0<t'<0.040$	1.68 ± 0.071	1.78 ± 0.071	135.6 ± 2.8
	Cu	$0<t'<0.025$	2.68 ± 0.11	2.75 ± 0.11	232.7 ± 4.3
	Ag	$0<t'<0.015$	3.44 ± 0.14	3.52 ± 0.14	306.5 ± 7.2
	Pb	$0<t'<0.015$	3.80 ± 0.16	3.87 ± 0.16	429.1 ± 13
1.2–1.4	C	$0<t'<0.040$	0.534 ± 0.040	0.599 ± 0.042	71.1 ± 2.3
	Al	$0<t'<0.040$	1.07 ± 0.043	1.18 ± 0.047	125.9 ± 2.6
	Cu	$0<t'<0.025$	1.57 ± 0.063	1.66 ± 0.067	202.3 ± 5.5
	Ag	$0<t'<0.015$	1.95 ± 0.078	2.01 ± 0.081	300.0 ± 3.9
	Pb	$0<t'<0.015$	2.19 ± 0.087	2.26 ± 0.090	387.6 ± 28
1.5–1.8	C	$0<t'<0.040$	0.334 ± 0.025	0.391 ± 0.028	63.6 ± 3.2
	Al	$0<t'<0.040$	0.642 ± 0.028	0.736 ± 0.030	111.9 ± 5.4
	Cu	$0<t'<0.025$	0.879 ± 0.035	0.959 ± 0.038	207.2 ± 13
	Ag	$0<t'<0.015$	1.03 ± 0.041	1.09 ± 0.044	264.4 ± 18
	Pb	$0<t'<0.015$	0.992 ± 0.040	1.05 ± 0.042	401.7 ± 44

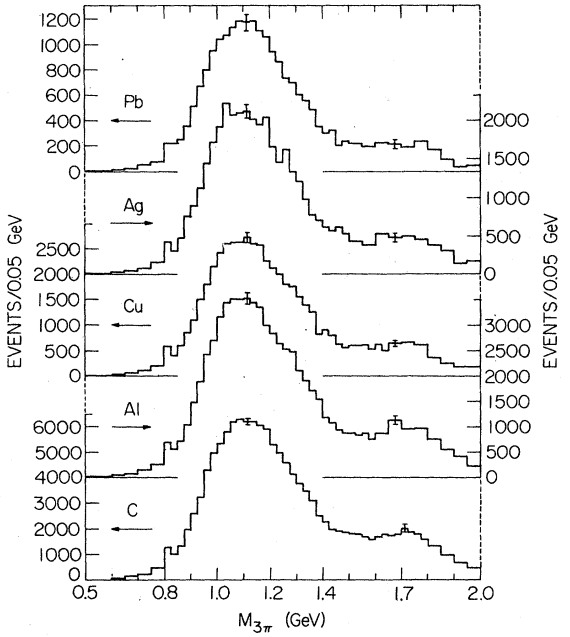

FIG. 2. Three-pion mass distributions for our five target nuclei, in the coherent region $0 < t' < 0.03$ GeV^2.

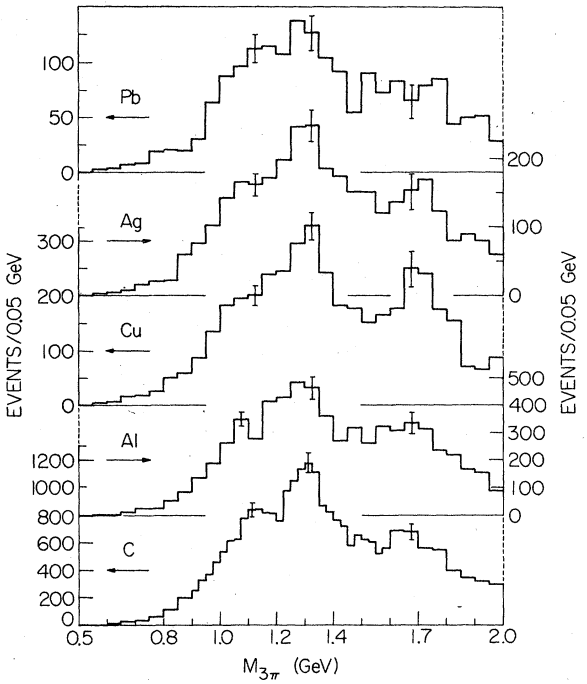

FIG. 3. Three-pion mass distributions for our five target nuclei, in the incoherent region $0.08 < t' < 0.40$ GeV^2.

duction; the momentum-transfer dependence, however, is completely different for the two cases. Indeed, in an experiment such as ours which does not measure the nuclear recoil, the only way to differentiate between the two types of production is by their t' distribution—the separation can only be statistically performed. Coherent production consists of a tall forward ($t' \to 0$) peak with diffraction maxima and minima trailing off to higher t', which move in to lower

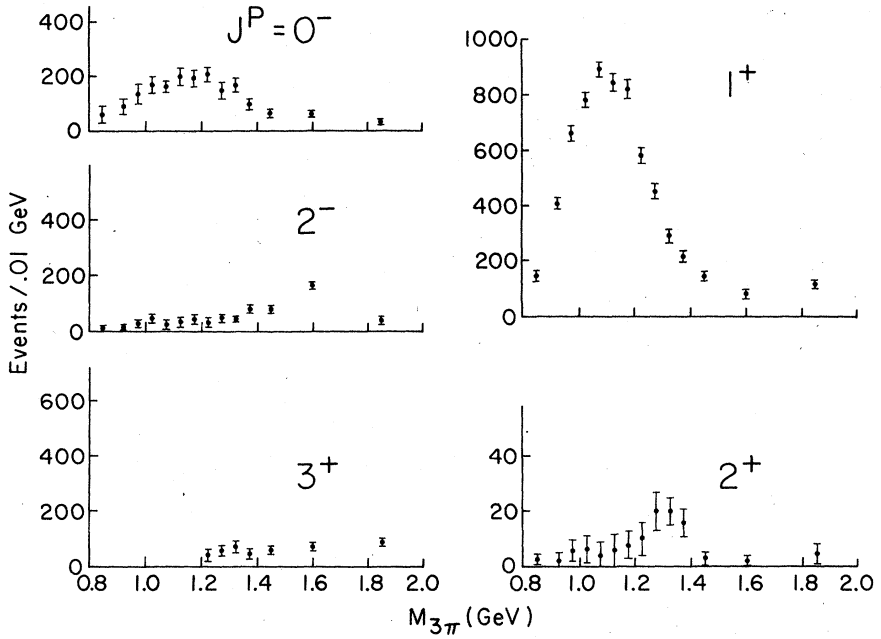

FIG. 4. Three-pion mass distributions for the important spin-parity states, for carbon in the region $0 < t' < 0.03$ GeV^2.

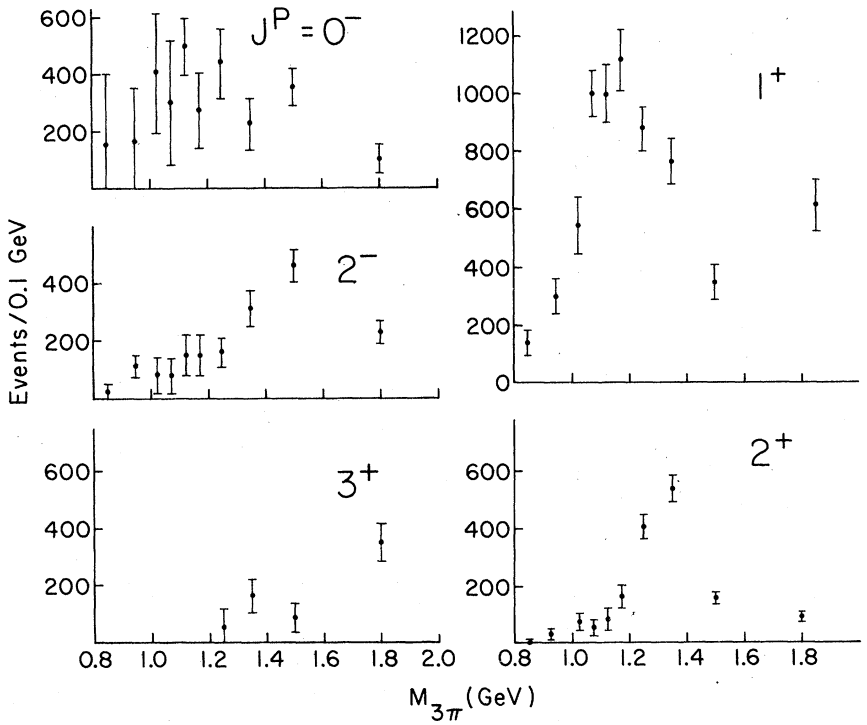

FIG. 5. Three-pion mass distributions for the important spin-parity states, for carbon in the region $0.08 < t' < 0.40$ GeV^2.

t' as A increases. Incoherent production has a t' dependence like that of the hydrogen data, and tends to mask the detailed coherent structure for the lighter nuclei; the second and third maxima are, however, visible in our highest nuclei.

Please note the application of the acceptance corrections to the data; the forward spectrometer efficiency is calculated within the partial-wave analysis, and all data points have been increased accordingly; the veto box efficiency has been independently calculated and has been used as a cut on the incoherent production of

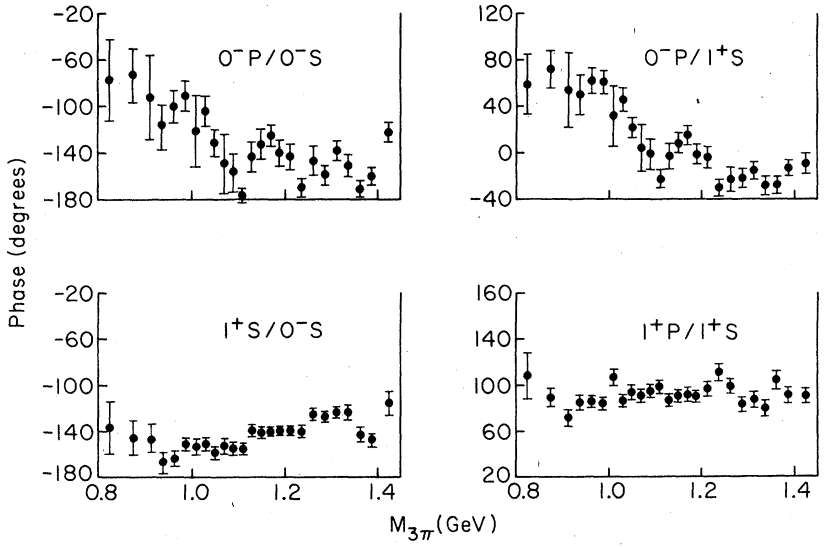

FIG. 6. The relative phases of some important spin-parity states, as a function of three-pion mass: C+Al+Cu+Ag, $0 < t' < 0.05$ GeV^2.

the model, so the data have not been corrected for this experimental bias. These remarks apply to all t' distributions throughout this work (and to all optical-model fits to the data).

As the forward spectrometer efficiency is practically independent of t', the raw distribution of the data can be corrected fairly accurately for the geometrical acceptance of the spectrometer. We took the correction factors determined in the partial-wave analysis as a function of t' and $M_{3\pi}$, and weighted each event accordingly. Figures 7, 8, and 9 show t' distributions for all target nuclei, in the A_1 ($1.0 < M_{3\pi} < 1.2$ GeV), A_2 ($1.2 < 1.4$ GeV), and A_3 ($1.5 < M_{3\pi} < 1.8$ GeV) regions. As only a few percent of the events are attributed to states with other than $M = 0$, our model for $M = 0$ is included in these figures.

The major contributing states with $M = 0$ are $J^P = 0^-$ and $J^P = 1^+$; their t' distributions are shown in Figs. 10 and 11, respectively. The coherent peaks all look alike because their structure is essentially determined by the size of the nucleus, and small differences in production from nucleons are masked by the nuclear size effects. The ratio of incoherent to coherent production does vary somewhat, reflecting the slightly different spin-parity composition at

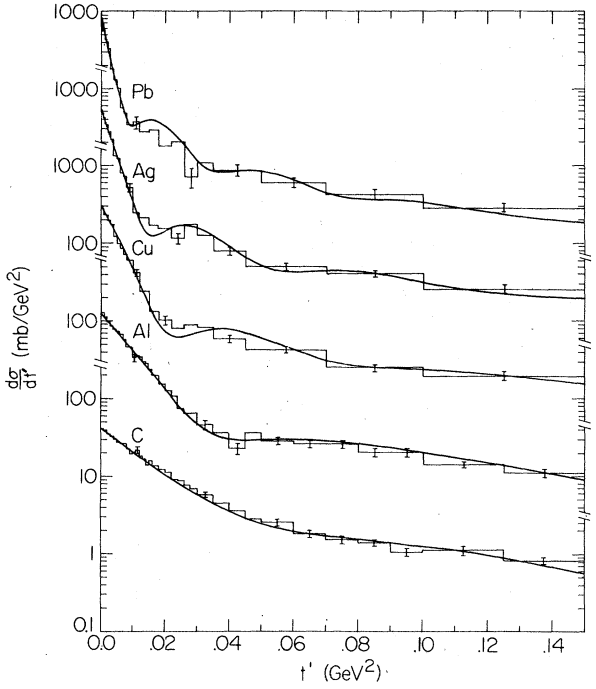

FIG. 8. t' distribution for our five target nuclei showing the total three-pion production in the A_2 region, $1.2 < M_{3\pi} < 1.4$ GeV.

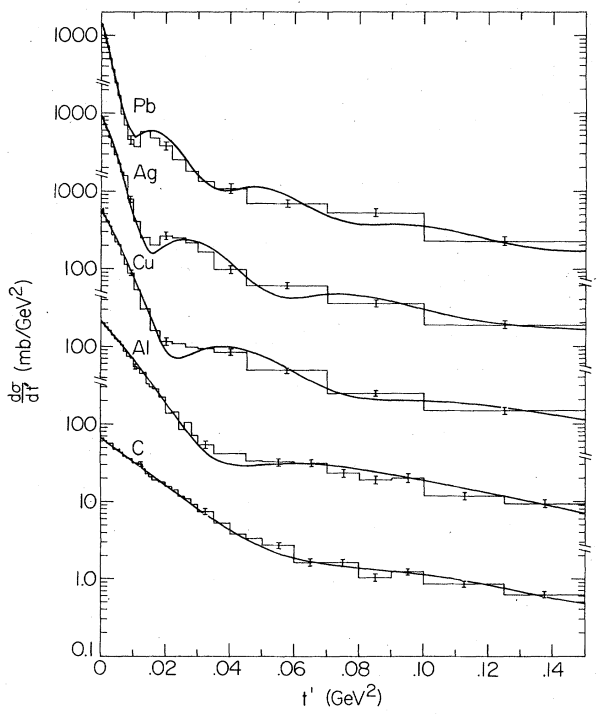

FIG. 7. t' distribution for our five target nuclei showing the total three-pion production in the A_1 region, $1.0 < M_{3\pi} < 1.2$ GeV.

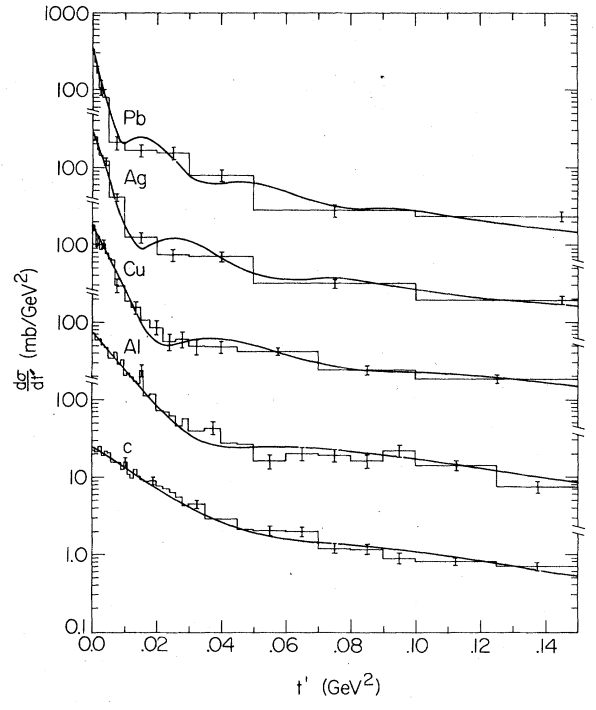

FIG. 9. t' distributions for our five target nuclei showing the total three-pion production in the A_3 region, $1.5 < M_{3\pi} < 1.8$ GeV.

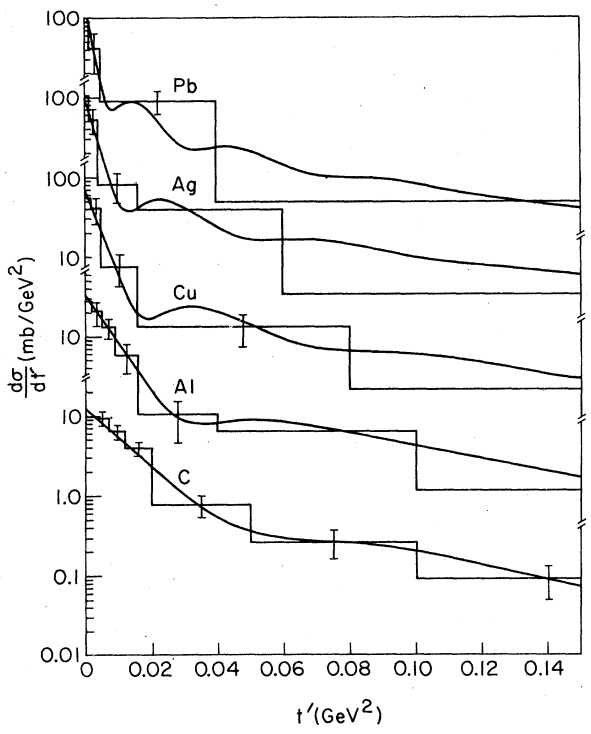

FIG. 10. t' distributions for $J^P = 0^-$, $1.0 < M_{3\pi} < 1.2$ GeV.

higher t'. The other $M = 0$ states [specifically the A_3 $(2^-S \to f\pi)$] have too low statistics to display in a meaningful way.

The only $|M| = 1$ wave of significance is the A_2, $2^+(D \to \rho\pi)1^+$, which is displayed in Fig. 12. Clearly present is the aforementioned forward dip in both the coherent and incoherent contributions.

D. *A* dependence

The A dependence of the coherent cross section is the determining factor for the absorption parameters of the model since the absorption is largest in the larger nuclei. In order to display this property, we have plotted a coherent cross section vs A for the various spin-parity states. The quantity plotted is the coherent $d\sigma/dt$ integrated over a single, wide, forward t' bin for each element. The cutoff in t' was chosen to contain approximately 90% of the coherent production (the bin width is therefore different for each element). In order to obtain data points for the individual spin-parity states, the incoherent/coherent ratio of the model for the total 3π production was assumed. The resulting incoherent subtractions were relatively small ($\lesssim$10%).

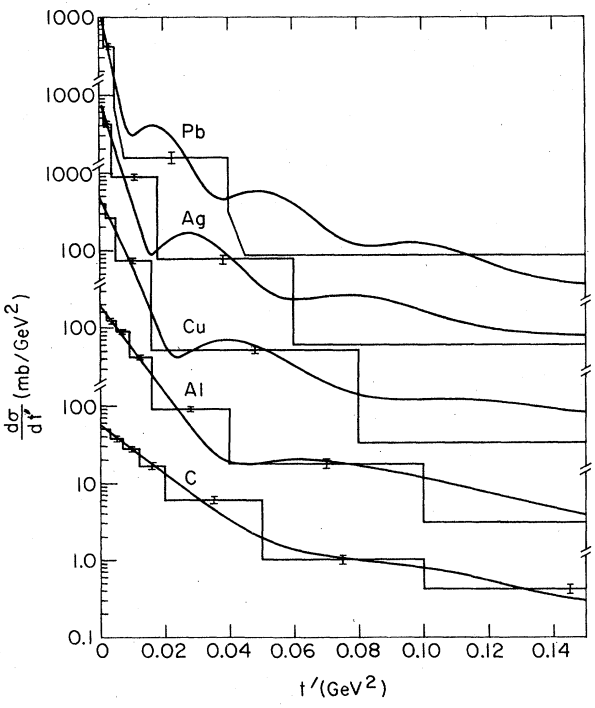

FIG. 11. t' distributions for $J^P = 1^+$, $1.0 < M_{3\pi} < 1.2$ GeV.

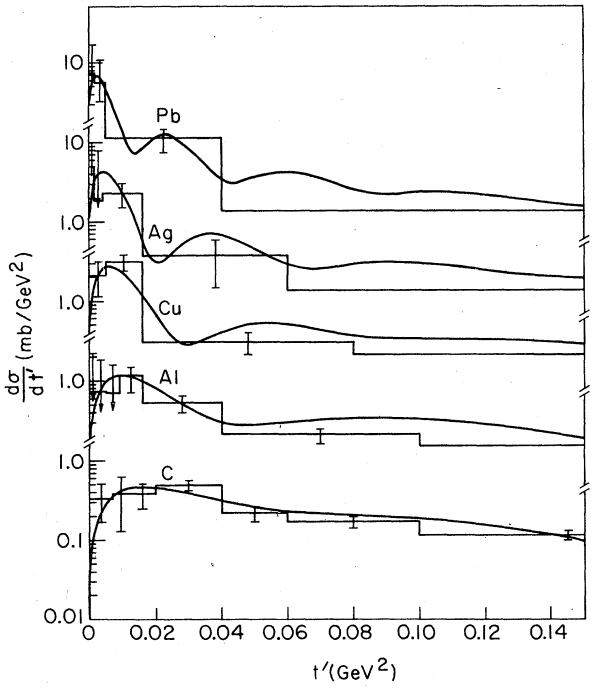

FIG. 12. t' distribution for $J^P = 2^+$, $|M| = 1$, $1.2 < M_{3\pi} < 1.4$ GeV.

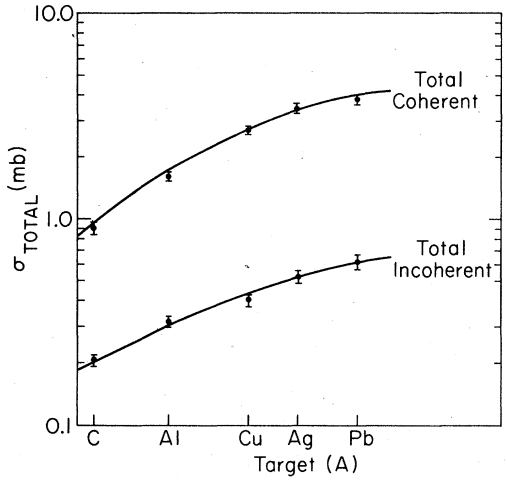

FIG. 13. The A dependence of the total coherent and incoherent three-pion production, $1.0 < M_{3\pi} < 1.2$ GeV.

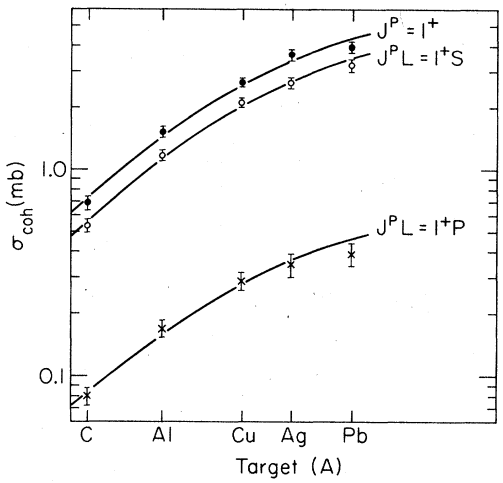

FIG. 15. The A dependence for coherent production of $J^P = 1^+$, $1.0 < M_{3\pi} < 1.2$ GeV.

These actual distributions are shown in Figs. 13–16, which show the total, 0^-, 1^+, and 2^- contributions to the production; the curves are the appropriate model fits.

The $|M| = 1$ state, $2^+(D \to \rho\pi)1^+$, has considerably more incoherent relative to coherent, because both are suppressed at small t', where the coherent would otherwise be completely dominant. Thus, the incoherent subtraction is more critical here than above. We have simply used the model's t' dependence for incoherent production, and used the same procedures as above. This distribution is shown in Fig. 17, with the model fit as before. Clearly, this incoherent subtraction is more model dependent than for the other states where the fraction of incoherent production is much smaller.

E. Other observations

The relative phases between some of the spin-parity states have been exhibited in Fig. 6 above, and they consistently show an excellent agreement with those observed in hydrogen. All comparable phases are, within the quoted errors, in complete agreement with those from Ref. 3. The A_1/A_2 phase is not very well determined because the A_2 $(2^+D \to \rho\pi)$ is itself small, and is suppressed in the forward direction where the A_1 is large. The general behavior of this phase, however, is consistent with the resonance character of the A_2 observed in hydrogen,[3] within statistical errors. The phases of the other small states are poorly determined, and the large errors make a comparison with hydrogen dif-

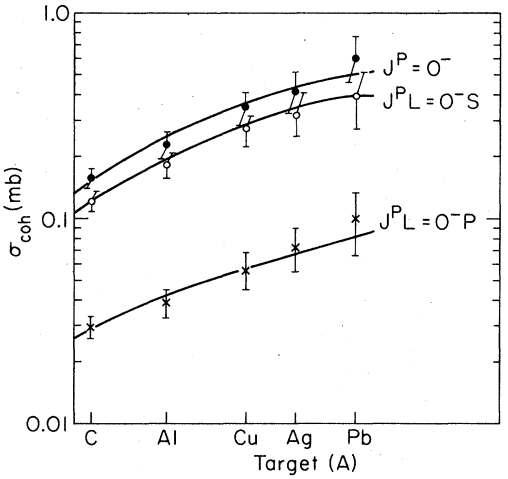

FIG. 14. The A dependence for coherent production of $J^P = 0^-$, $1.0 < M_{3\pi} < 1.2$ GeV.

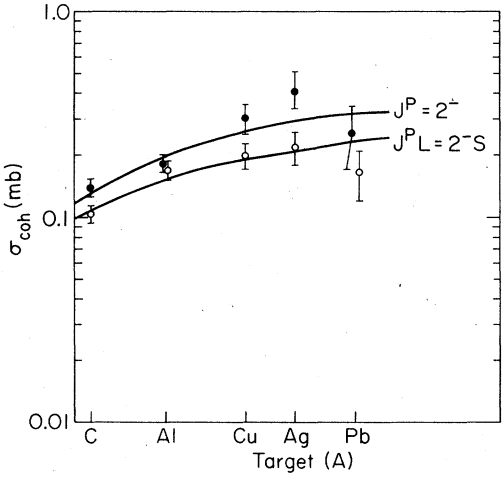

FIG. 16. The A dependence for coherent production of $J^P = 2^-$, $1.5 < M_{3\pi} < 1.8$ GeV.

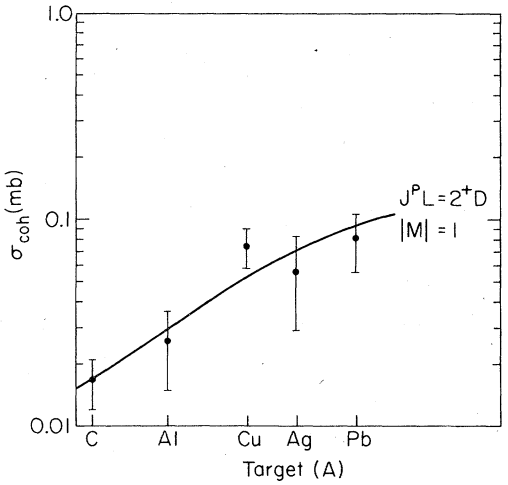

FIG. 17. The A dependence for coherent production of $J^P = 2^+$, $|M| = 1$, $1.2 < M_{3\pi} < 1.4$ GeV.

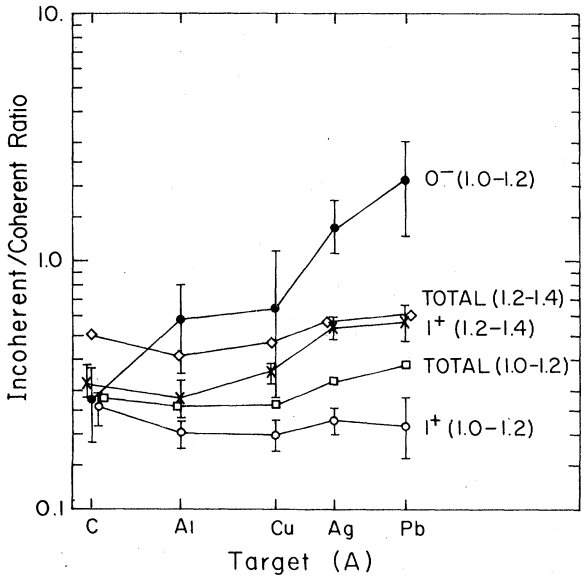

FIG. 18. The A dependence of the incoherent /coherent ratios for several spin-parity states, from double-exponential fits to the data.

ficult.

In order to study the ratios of the incoherent cross section to the coherent cross section, we have done a series of fits using a double-exponential parametrization similar to that of Ref. 1, but using the ratio of incoherent to coherent as a parameter rather than the incoherent cross section (to make error calculation easy). These results are shown in Fig. 18, where the ratio of the total incoherent cross section to the total coherent cross section is plotted vs A for several states. The ratios for the $J^P = 1^+$ state all stay between 0.2 and 0.7, as do the ratios for the total three-pion production. But the $J^P = 0^-$ ratio increases with A by almost a full order of magnitude (0.27 to 2.1). Although the errors are large, this is a significant difference. We did not include the smaller states ($J^P = 2^-$ and $J^P = 3^+$) in the figure because their errors are very large, but they too remain fairly constant, and less than 0.8. Both $0^-(S \to \epsilon\pi)$ and $0^-(P \to \rho\pi)$ increase dramatically with A, although the latter is not very well measured; both $1^+(S \to \rho\pi)$ and $1^+(P \to \epsilon\pi)$ have this ratio below 0.5 for all A.

This behavior of the $J^P = 0^-$ wave is due to one simple cause: The increase with A of the coherent production is smaller for 0^- than for any other J^P state. The increase with A of the incoherent production is the same for 0^- as for the other states. The increase of the incoherent/coherent ratio with A is then a consequence of the abnormal A dependence of the 0^- coherent production.

IV. OPTICAL MODEL FOR THREE-PION PRODUCTION

The basic ideas and derivation of the high-energy optical model have been given in Glauber's classic papers,[4] and have been specifically extended to apply to inelastic final states by Kölbig and Margolis.[6] Our treatment differs from theirs by including the effects of a helicity change in A_2 production.

The assumptions used in the model are as follows:

(1) The 3π system is produced upon a single nucleon, at a definite point.

(2) The interaction with the nucleus of the incoming (π) and outgoing (3π) waves can be treated in an eikonal approximation, with the nucleus treated as a continuous absorber. The incoming wave is assumed to remain a pion up to the $\pi \to 3\pi$ interaction, and the quantum numbers of the outgoing wave are also assumed to be unchanged after that interaction.

(3) The scattering angle is small, so interactions with the nucleus can be approximated by the scattering in the forward direction, and the path traveled through the nucleus by a straight line.

(4) Nuclear correlations are negligible, we can use a Woods-Saxon parametrization of the nuclear density, and interactions with neutrons and protons are the same.

Assumption (1) is open to question because it does not account for the cascade-type processes which may contribute, and assumption (2) ignores the production of intermediate states which may then interact with the nucleus to produce a three-pion state. These assumptions, do however, yield

a framework within which realistic calculations can be made.

We assume the amplitude for production on bare nucleons (hydrogen) is known; multiplying it by the nuclear density (at a given point) then gives the amplitude for production on a given nucleon at that point. Summing over all nucleons, and integrating over the nuclear volume then gives the amplitude for nuclear production. There are two cases normally considered: (1) the nucleus remains in its ground state, and (2) the nucleus is excited or breaks up (i.e., does not remain in its ground state). As the nuclear density function is directly related to the ground-state wave function, we sum over all possible final states and use closure in order to calculate the cross section. The first case (ground state) is called *coherent production*, because the amplitudes for production on individual nucleons add coherently; the second case (excited or broken nucleus) is called *incoherent production*, because this cross section is essentially a sum of the squares of the amplitudes for production on the individual nucleons. The results of the derivation[7] are

$$\left.\frac{d\sigma}{dt}\right|_A(\vec{q}) = \left.\frac{d\sigma}{dt}\right|_{\substack{\text{bare}\\ \text{nucleons}}}(\vec{q})[A(A-1)|\tilde{F}_A(\vec{q})|^2 + AN_A(\vec{q})], \tag{4.1}$$

$$|\tilde{F}_A(\vec{q})|^2 = \left| \int d^3r\, \rho_A(\vec{r}) \times \{e^{i\vec{q}\cdot\vec{r}} \exp[-\tfrac{1}{2}\tilde{\sigma}_1 T_1(\vec{r})] \times \exp[-\tfrac{1}{2}\tilde{\sigma}_2 T_2(\vec{r})]\}\right|^2, \tag{4.2}$$

$$N_A(q) = \int d^3r\, \rho_A(\vec{r}) \times \left| \{e^{i\vec{q}\cdot\vec{r}} \exp[-\tfrac{1}{2}\tilde{\sigma}_1 T_1(\vec{r})] \times \exp[-\tfrac{1}{2}\tilde{\sigma}_2 T_2(\vec{r})]\}\right|^2, \tag{4.3}$$

where $\vec{q}$ = momentum transfer, $\rho_A(\vec{r})$ = nucleon density function, the thickness functions are

$$T_1(\vec{r}) = A\int_{-\infty}^{z} dz\, \rho_A[(x^2+y^2+z^2)^{1/2}],$$
$$T_2(\vec{r}) = A\int_{z}^{\infty} dz\, \rho_A[(x^2+y^2+z^2)^{1/2}], \tag{4.4}$$

and the absorption parameters $\tilde{\sigma} = \sigma(1 - i\alpha)$ come from the elastic interaction of the waves with the (continuous) nuclear matter via the optical theorem: σ = total interaction cross section, α = real to imaginary ratio of the corresponding forward elastic amplitude.

The physical interpretation of this formula is straightforward: $T_1(\vec{r})$ is merely the total amount of nuclear matter traversed by the incoming pion, so the phase change of the incident wave is

$$\exp\left(\frac{-2\pi i}{k} f(0)\, T_1(\vec{r})\right),$$

with a similar expression for the outgoing wave. These "distorted-wave" factors multiply the usual $e^{i\vec{q}\cdot\vec{r}}$ which is the phase difference of the two plane waves (because of the momentum transfer). Multiplying these phase factors by the amplitude for production at a given point,

$$\left(\left.\frac{d\sigma}{dt}\right|_{\substack{\text{bare}\\ \text{nucleons}}}(\vec{q})\right)^{1/2} \rho_A(\vec{r}),$$

and then integrating over all space, you obtain the above formula. Note that we are ignoring the unknown phase in the production from bare nucleons.

In order to exhibit the coherent and incoherent production more clearly, Fig. 1 shows a model calculation for silver, and the separate contribution of coherent and incoherent production. The parameters used in this calculation come from a five-element fit to the data, described in Sec. V.

For A_2 production, the helicity change at the meson vertex requires that the amplitude vanish in the forward direction as $|\vec{q}|$—this can be directly incorporated into the formalism

$$\left.\frac{d\sigma}{dt}\right|_A^{A_2}(\vec{q}) = \left.\frac{d\sigma^0}{dt}\right|_{\substack{\text{bare}\\ \text{nucleons}}}^{A_2}(\vec{q})[A(A-1)|\tilde{F}'_A(\vec{q})|^2 + AN'_A(\vec{q})], \tag{4.5}$$

$$|\tilde{F}'_A(\vec{q})|^2 = \left| \int d^3r\, \rho_A(\vec{r}) \times \frac{d}{dx}\{e^{i\vec{q}\cdot\vec{r}} \exp[-\tfrac{1}{2}\sigma_1 T_1(\vec{r})] \times \exp[-\tfrac{1}{2}\sigma_2 T_2(\vec{r})]\}\right|^2, \tag{4.6}$$

$$N'_A(\vec{q}) = \int d^3r\, \rho_A(\vec{r}) \times \frac{d}{dx}\left| e^{i\vec{q}\cdot\vec{r}} \exp[-\tfrac{1}{2}\sigma_1 T_1(\vec{r})] \times \exp[-\tfrac{1}{2}\sigma_2 T_2(\vec{r})]\right|^2. \tag{4.7}$$

Here we have used a reduced cross section

$$\left.\frac{d\sigma^0}{dt'}\right|_{\substack{\text{bare}\\ \text{nucleon}}}^{A2} = \frac{1}{t'}\left.\frac{d\sigma}{dt'}\right|_{\substack{\text{bare}\\ \text{nucleon}}}^{A_2}, \tag{4.8}$$

which does not vanish in the forward direction, and $\hat{x}$ is the direction of the perpendicular component of the momentum transfer $\vec{q}$.

By integrating the formula for $|\tilde{F}'_A(q)|^2$ by parts, we see that $|\tilde{F}'_A(q)|^2$ for A_2 production ($|M| = 1$)

is proportional to the derivative of $\rho_A(r)$, and is therefore largest on the edge of the nucleus. For production without helicity change $|\vec{F}_A(\vec{q})|^2$ is proportional to $\rho_A(r)$, and is largest in the center of the nucleus.

The cross section naturally divides into the two usual pieces—the A^2 term describes coherent production, while the two terms proportional to A comprise the incoherent part.

The production on bare nucleons is assumed to be the same as that on hydrogen, which is parametrized[8]

$$\left.\frac{d\sigma}{dt}\right|_{\substack{\text{bare}\\\text{nucleons}}}(\vec{q}) = (q_\perp^2)^M \left.\frac{d\sigma^0}{dt}\right|_{\substack{\text{bare}\\\text{nucleons}}}(\vec{q}) \equiv (t')^M \left.\frac{d\sigma^0}{dt}\right|_{\substack{\text{bare}\\\text{nucleons}}}(\vec{q}) = (t')^M C_0 e^{-bt'}, \tag{4.9}$$

where C_0 and b are both dependent upon $M_{3\pi}$.

The nucleon density function is parametrized[9]

$$\rho_A(r) = \frac{\rho_0}{1+e^{(r-\rho_1)/\rho_2}}, \qquad \frac{1}{\rho_0} = \int \frac{d^3r}{1+e^{(r-\rho_1)/\rho_2}}. \tag{4.10}$$

In applying this model to the data, we quickly discovered problems in the incoherent region—the model was a factor of 2 to 3 times too large. We feel that this discrepancy is associated with the vetoing of incoherent events by the target veto box. For incoherent events, particles and γ rays emerging from the target can veto the event. We have tried to obtain a crude estimate $\epsilon_A(\vec{q})$ for the efficiency of observing an incoherent event with momentum transfer $\vec{q}$, and target element A. The uncertainties associated with real incoherent production are so large that we feel we cannot obtain a reliable estimate of the effect of the target veto box. We therefore assumed that the $\vec{q}$ dependence of this acceptance is proportional to our simple calculations, and have added an extra parameter I_A for each element, which multiplies $\epsilon_A(\vec{q})$. This "incoherent ratio" parameter gives a measure of the experimental incoherent cross section relative to our optical-model calculation multiplied by our crudely estimated acceptance $\epsilon_A(\vec{q})$.

Thus, the actual formula fitted to the data is

$$\left.\frac{d\sigma}{dt}\right|_A(\vec{q}) = \left.\frac{d\sigma}{dt}\right|_{\substack{\text{bare}\\\text{nucleon}}}(\vec{q})\{A^2|\tilde{F}_A(\vec{q})|^2 + A[I_A\epsilon_A(\vec{q})] \times [N_A(\vec{q}) - |\tilde{F}_A(\vec{q})|^2]\}, \tag{4.11}$$

where $\epsilon_A(q)$ is our calculated efficiency for detecting incoherent events, and the effect of our resolution in $\vec{q}$ has not been shown. For a fit to our five elements there are nine parameters: C_0, b, σ_2, α_2, I_C, I_{Al}, I_{Cu}, I_{Ag}, I_{Pb}. The status of these parameters in the various fits is listed in Table IV, which also gives the values of our nuclear density parameter ρ_1 and ρ_2, and our resolution in transverse momentum transfer $\sigma_{q_\perp}$.

We have performed two types of fits to the data. Type I fits include data from the entire t' range of the experiment. Typically we used four to eight t' bins for each element when analyzing partial-wave results, and many more bins per element when fitting the total 3π production. Type II fits used one bin per element representing the total coherent production, as explained in Sec. III D.

V. OPTICAL-MODEL RESULTS

In this section we present the values of parameters which result from fitting the optical-model formulas of Sec. IV to the results of Sec. III. In Sec. V A we discuss the 3π absorption parameters σ_2 and α_2, and in Sec. V B we discuss the hydrogen production parameters C_0 and b.

These fits of model to data have been illustrated above in Figs. 7–17, which show the t' and A dependence of both model and data. In these fits, all known efficiencies are included, as is the experimental resolution in $q_\perp$. In general, the agreement between the model curves and the

TABLE IV. Model parameters.

(a) Values independent of A

	Type I fits to PWA	Type I fits to total 3π	Type II fits
σ_1 (mb)	25.0	25.0	25.0
α_1	0.0	−0.15	0.0
σ_2	a	a	a
α_2	0.0	a	0.0
C_0	a	a	a
b (GeV^{-2})	9.5	a	9.5

(b) Values dependent upon A

	I_A	ρ_1 (fm)	ρ_2 (fm)	$\sigma_{q_\perp}$ (GeV)
carbon	b	2.31	0.471	0.0108
aluminum	b	3.24	0.478	0.0103
copper	b	4.41	0.450	0.0145
silver	b	5.42	0.425	0.0147
lead	b	6.78	0.460	0.0168

[a] Variable parameter in fit.
[b] Variable in type I fits, ignored in type II fits.

data is quite good. Note, however, that the fit in the incoherent region is not really significant since the magnitude in this region is adjusted by the parameters I_A, as mentioned above. The actual experimental data are plotted; the curves are from calculations with the optical model, with the incoherent contribution multiplied by $I_A \epsilon_A(\tilde{q})$ as explained in Sec. IV.

A. Absorption parameters σ_2 and α_2

The three-pion absorption parameters, σ_2 and α_2, are really the most interesting parameters of the model since one can consider them as describing the total "$(3\pi)+N \rightarrow$ anything" cross section and the real to imaginary ratio of the corresponding elastic amplitude. Unfortunately,

TABLE V. Absorption parameters.

$M_{3\pi}$ region (GeV)	State	σ_2 (mb)	α_2
1.0–1.2	Total	$24.88^{+0.85}_{0.82}$	-0.500 ± 0.035
	0^-(all decays)	60.22^{+15}_{12}	
	$0^-(S \rightarrow \epsilon\pi)$	60.11 ± 4.5	
	$0^-(P \rightarrow \rho\pi)$	120.2 ± 35	
	1^+(all decays)	$25.37^{+1.1}_{1.1}$	
	$1^+(S \rightarrow \rho\pi)$	26.14 ± 0.97	
	$1^+(P \rightarrow \epsilon\pi)$	26.15 ± 2.4	
1.2–1.4	Total	$22.79^{+1.3}_{1.2}$	-0.554 ± 0.026
	0^-(all decays)	$29.75^{+5.0}_{4.2}$	
	$0^-(S \rightarrow \epsilon\pi)$	42.73 ± 7.5	
	$0^-(P \rightarrow \rho\pi)$	22.05 ± 1.6	
	1^+(all decays)	$24.28^{+1.7}_{1.7}$	
	$1^+(S \rightarrow \rho\pi)$	27.74 ± 0.9	
	$1^+(P \rightarrow \epsilon\pi)$	35.26 ± 8.2	
	2^-(all decays)	$25.30^{+8.5}_{7.5}$	
	3^+(all decays)	$19.46^{+6.2}_{5.1}$	
	$2^+(D \rightarrow \rho\pi)1^+$	29.12^{+34}_{18}	
1.5–1.8	Total	$18.89^{+1.85}_{1.85}$	-0.606 ± 0.043
	0^-(all decays)	51.27^{+33}_{17}	
	1^+(all decays)	79.02^{+50}_{27}	
	2^-(all decays)	74.34^{+50}_{28}	
	3^+(all decays)	$21.18^{+8.2}_{6.2}$	

most of this discussion will ignore α_2, because the data are usually incapable of determining it.

The fit results for σ_2 are given in Table V, for all important partial waves, and for the total three-pion production; these values came from the type I fits of Fig. 14–18, and similar ones not illustrated. A brief inspection shows that, with the exception of $J^P = 0^-$, the absorption cross sections are roughly 25 mb, the value for the absorption of single pions.

These absorptions have proved to be puzzling indeed, and their interpretation remains unclear. It is easy to show that for three uncorrelated, mutually noninteracting pions the absorption should be $3 \times 25 = 75$ mb; somewhat less when shadowing is taken into account, perhaps as low as 50 mb.[10] It is very tempting to point to these absorptions and claim that they "prove" that the 3π system acts as a single particle within the nucleus. Reinforcing this claim are simple calculations of the lifetimes of the A_1, A_2, and A_3 mesons from their mass widths—these indicate that all three mesons would nominally travel several nuclear diameters between their production and decay. In this picture, then, the 0^- is not a particle, so it naturally suffers a higher absorption because it is really several objects traveling together. It remains unclear, however, why the nonresonant A_1 and A_3 ($1^+S \to \rho\pi$ and $2^-S \to f\pi$), which may or may not be due to a Deck-type mechanism,[11] act in this sense as single particles. These naive ideas are expanded upon by Gottfried,[12] noting that the meson system may travel many nuclear diameters while still reacting to the impact with the nucleus (and characterized only by an energy flux, not as ordinary hadrons).

Another point is to observe that even for three separate pions produced at the front of the nucleus, the three particles would be within 0.3 F or so of each other at the rear of the nucleus, so that all three would tend to concentrate on the same nucleons. In other words, "one pion drills a hole (in the nucleus), and the others follow."[13] In this picture it is difficult to predict what the absorption should be, as there is no way to know how well they follow the leader.

A still different point is to note that as the three-pion system propagates through the nucleus, reinteractions can change the basic properties of that system (mass, spin, etc.). In this picture, the results depend upon the detailed structure of the reinteractions, of which we have no direct experimental knowledge. Sample calculations have shown that the observed low absorptions can be obtained with suitable care.[14]

In short, there is no definitive explanation for these low absorptions, at present. As we shall see in the next section, this situation is not unique to three-pion final states, and appears consistently in the study of many kinds of hadronic interactions within nuclear targets.

The absorption cross section of the total 3π system (shown in Table V) decreases steadily with increasing 3π mass. In a study of the reaction $pA \to p\pi^+\pi^-A$ (Ref. 15) the absorption cross section of the $p\pi^+\pi^-$ system shows a similar decrease with increasing $p\pi^+\pi^-$ mass.

The measurement of α_2 can be done well only for the total three-pion production. The values obtained are also exhibited in Table V, and are somewhat larger than those found in stable hadron-nucleon elastic processes, such as πp and kp elastic scattering (which are roughly -0.15), but are similar to those found in an analysis of $p\pi\pi$ production on nuclei[15] (they find -0.5 ± 0.2).

B. Normalization parameters C_0

The overall normalization parameters C_0 and the fitted coefficient in the exponential b are shown in Table VI for the three mass regions. The coefficient b was fitted only to the total production. We also show for comparison corresponding values from hydrogen data for the total production, $1^+(S \to \rho\pi)$, and $2^+(D \to \rho\pi)$ states, corrected to 22.6 GeV/c. As mentioned earlier, the agreement for C_0 is quite good, but the nuclear values for b are consistently lower than those from hydrogen data. The nuclear values for b are determined primarily in the incoherent region, where our systematic errors are large. The errors quoted are statistical only.

For fits to individual partial waves, b could not be well determined, due to large statistical errors in the high-t' bins. Instead, a value of $b = 9.5$ GeV^{-2} was used for all such fits.

C. Fit backgrounds and stabilities

We have investigated the stability of the values for σ_2 obtained in fitting the data. This investigation was performed primarily for fits to the total three-pion production (because of the large statistics available), but these tests were also performed on fits to 0^- (total) and 1^+ (total) as well.

Since the values of σ_2 are determined primarily in the coherent production region, the principal background problem comes from the incoherent production in this low-t' region. We have used the model to extrapolate the incoherent production to low t' and therefore we investigated the effect of changing the dip structure in the forward direction predicted by the model. We doubled the magnitude of the dip, removed the dip completely (so that $d\sigma/dt$ is a simple exponential for the

TABLE VI. Production parameters. Errors are statistical only.

$M_{3\pi}$ region (GeV)	State	C_0 (mb/GeV^2)	b (GeV^{-2})	Values from hydrogen data C_0 (mb/GeV^2)	b (GeV^{-2})
1.0–1.2	Total	1.404 ± 0.033	7.160 ± 0.106	1.32 ± 0.16	11.0 ± 1
	0^-(all decays)	0.451 ± 0.115			
	$0^-(S \to \epsilon\pi)$	0.394 ± 0.025			
	$0^-(P \to \rho\pi)$	0.208 ± 0.092			
	1^+(all decays)	1.171 ± 0.016			
	$1^+(S \to \rho\pi)$	0.946 ± 0.043		1.11 ± 0.19	12.1 ± 1.1
	$1^+(P \to \epsilon\pi)$	0.126 ± 0.010			
1.2–1.4	Total	0.851 ± 0.013	5.656 ± 0.134	1.02 ± 0.15	8 ± 1
	0^-(all decays)	0.230 ± 0.032			
	$0^-(S \to \epsilon\pi)$	0.194 ± 0.034			
	$0^-(P \to \rho\pi)$	0.061 ± 0.003			
	1^+(all decays)	0.542 ± 0.032			
	$1^+(S \to \rho\pi)$	0.471 ± 0.019		0.472 ± 0.081	8.0 ± 1.0
	$1^+(P \to \epsilon\pi)$	0.089 ± 0.020			
	2^-(all decays)	0.073 ± 0.018			
	3^+(all decays)	0.069 ± 0.005			
	$2^+(D \to \rho\pi)\lvert M\rvert=1$	1.085 ± 0.293		1.08 ± 2.9	8.5 (fixed)
1.5–1.8	Total	0.583 ± 0.008	4.663 ± 0.188	0.754 ± 0.144	6.5 ± 1
	0^-(all decays)	0.244 ± 0.022			
	1^+(all decays)	0.699 ± 0.117			
	2^-(all decays)	0.547 ± 0.226			
	3^+(all decays)	0.166 ± 0.012			

incoherent production), and also introduced a forward peak (equal in magnitude to the dip) in the incoherent cross section. None of these alterations changed the fitted values of σ_2 significantly. We also investigated the effect of changing the values of the parameters $\{I_A\}$. When we doubled the values of $\{I_A\}$, we did significantly increase the χ^2 values for the fits, but the values of σ_2 stayed within 0.5 standard deviations of the previous fitted values.

We also examined the effects of varying the other parameters in the fit. Only the normalization parameter C_0 had a strong effect on the fitted value for σ_2. C_0 was always left as an adjustable parameter in the fit; in a simplified picture, the small A targets then set C_0 and the large A elements determined σ_2 for this C_0. Thus although there can be questions about normalizing this experiment to hydrogen experiments, the C_0 in each fit is determined from this experiment alone, and we expect no systematic effects on σ_2. Variation of the slope parameter b produced effects similar to those from variation of the parameters $\{I_A\}$, and did not affect σ_2 significantly. Also the experimental resolution in $q_\perp$ affects χ^2 strongly without affecting σ_2. Removing the estimate for the veto box $\epsilon_A(\vec{q})$ affects the slope parameter b since both describe the t' dependence of the incoherent cross section. Again the values of σ_2 were not changed significantly.

VI. CONCLUSIONS

Our principal results on production cross sections for the various target nuclei have been summarized in Table III and in Figs. 7–17. We summarize some conclusions from these results below:

Partial-wave structure

The partial-wave analysis of these nuclear data is strikingly similar to that of the hydrogen data. Except for the momentum-transfer dependence, which is strongly influenced by the size of the target nucleus, virtually all properties of the hydrogen data remain. The list of mesons is the same (A_1, A_2, A_3'), the appearance of dipion resonances in the π^+-π^- mass spectra is similar (ϵ^0, ρ^0, f^0), the relative importance of the spin-parity states is about the same (1^+S dominates, etc.), and their phases behave as in hydrogen (the A_2 is resonant, all others are not).

The optical model works fairly well

We find that the optical model of Sec. IV works quite well in describing the coherent three-pion

production on nuclei; the model does not agree with the data for incoherent production.

This experiment was designed to trigger on coherent production only; it is therefore extremely difficult to estimate the acceptance in the experimental data for incoherent production. We believe this uncertainty in the trigger is the primary reason for the disagreement between the model and the experimental cross sections in the incoherent region.

In any case, the consistent observation of two distinct t' structures in all kinds of nuclear production of hadrons makes it seem quite likely that any successful model for such processes must contain both coherent and incoherent parts, in a manner similar to these optical models.

The A_2 is coherently produced

Again, we mention our observation of coherent production of the A_2 meson ($2^+ D \to \rho\pi$). This adds to the list of evidence for the exchange of a Pomeron contributing to this production[8]:

1. P_{lab} dependence in hydrogen suggests a Regge trajectory intercept greater than 0.7.
2. The exchanged object has natural parity [i.e., $P = (-1)^{\text{spin}}$] and isospin zero.
3. The A_2 is produced coherently in nuclei.

The coherent nuclear production of both the A_1 and the A_2, and the strong interference of their amplitudes, strengthens the conclusion that they are both produced predominantly by a nonflip of the nucleon spin.

Optical-model absorption cross sections

We find that the optical-model absorption in nuclear matter of the produced three-pion system is roughly equal to the absorption of a single pion (25 mb), for practically any subset of the data. The major exception is the $J^P = 0^-$ component, which is absorbed with a cross section of roughly 50 mb. These results are consistent with similar analyses of other experiments on particle production on nuclei. Optical-model analyses of such experiments generally find these absorption cross sections to be considerably smaller than the sum of the (known) cross sections for the outgoing final particles, and, except for photoproduction, obtain results commensurate with the absorption of the beam particle. The absorption of the 0^- state is below the naive expectation of 75 mb, but is also considerably above the beam absorption (25 mb). The 3π $J^P(0^-)$ is then the first system in production by hadrons to have an absorption appreciably larger than the absorption of the incident particle. Our result on this 0^- system is in good agreement with the result given in Ref. 16. At this writing, there appears to be no quantitative theoretical accounting for these optical-model absorptions in nuclear matter.

ACKNOWLEDGMENTS

We are grateful to the Lindenbaum-Ozaki group, who constructed and helped maintain the Mark I spectrometer facility at Brookhaven National Laboratory. We wish to thank our colleagues G. Ascoli, D.G. Ravenhall, and R.S. Schult for their advice, both in the partial-wave analysis and in the application of the optical model. This work was supported in part by the U.S. Energy Research and Development Administration.

---

*Present address: University of Michigan, Ann Arbor, Mich. 48103.

†Present address: Elscint Inc., Palisades Park, N. J., 07650.

‡Present address: General Automation, Anaheim, Calif., 92800.

¶Present address: Stanford Linear Accelerator Center, Stanford, Calif., 94305.

[1]U. E. Kruse, T. J. Roberts, R. M. Edelstein, E. J. Makuchowski, C. M. Meltzer, E. L. Miller, J. S. Russ, B. Gobbi, J. L. Rosen, H. A. Scott, S. L. Shapiro, and L. Strawczynski, Phys. Rev. Lett. 32, 1328 (1974).

[2]K. J. Foley, W. A. Love, S. Ozaki, E. D. Platner, A. C. Saulys, E. H. Willen, and S. J. Lindenbaum, Nucl. Instrum. Methods 108, 33 (1973); see also Ref. 15.

[3]G. Ascoli *et al.*, Phys. Rev. D 7, 669 (1973); G. Ascoli *et al.*, Phys. Rev. Lett. 26, 929 (1971); and references therein; Ref. 8; Yu. M. Antipov *et al.*, Nucl. Phys. B63, 141 (1973); B63, 153 (1973); R. Klanner, Ph.D. thesis, Univ. of Munich, Germany, 1973 (unpublished).

[4]R. J. Glauber, in *Lectures in Theoretical Physics*, edited by W. E. Brittin and L. G. Dunham (Interscience, New York, 1959), p. 315; in *High Energy Physics and Nuclear Structure*, edited by G. Alexander (North-Holland, Amsterdam, 1967), p. 311; in *High Energy Physics and Nuclear Structure*, edited by S. Devons (Plenum, New York, 1970), p. 311.

[5]V. A. Karmanov and L. A. Kondratyuk, Zh. Eksp. Teor. Fiz. Pis'ma Red. 18, 451 (1973) [JETP Lett. 18, 266 (1973)]; A. B. Kaidalov and L. A. Kondratyuk, Nucl. Phys. B56, 90 (1973); J. Pumplin and M. Ross, Phys. Rev. Lett. 21, 1778 (1968).

[6]K. S. Kölbig and B. Margolis, Nucl. Phys. B6, 85 (1968).

[7]T. J. Roberts, Ph.D. thesis, Univ. of Illinois, 1975

(unpublished).
[8]G. Ascoli *et al.*, Univ. of Illinois report (unpublished).
[9]The nuclear density parameters ρ_1 and ρ_2 which are displayed in Table IV come from a Harteee-Fock calculation which fitted nucleon densities to electron scattering data. We wish to thank D. G. Ravenhall for these results.
[10]R. T. Cutler (private communication).
[11]G. Ascoli, R. Cutler, L. M. Jones, U. Kruse, T. Roberts, B. Weinstein, and R. W. Wyld, Jr., Phys. Rev. D 9, 1963 (1974); G. Ascoli, L. M. Jones, B. Weinstein, and H. W. Wyld, Jr., *ibid.* 8, 3894 (1973).
[12]K. Gottfried, Acta Phys. Pol. B3, 769 (1972); K. Gottfried, contributed paper to APS Meeting, Washington D.C., 1975 (unpublished).
[13]G. Ascoli (private discussion).
[14]L. Van Hove, Nucl. Phys. B46, 75 (1972); in *High Energy Physics and Nuclear Strucutre*, Proceedings of the Fifth International Conference, Uppsala, Sweden, 1973, edited by G. Tibell (North-Holland, Amsterdam/American Elsevier, New York, 1974), p. 109.
[15]E. J. Makuchowski, Ph.D. thesis, Carnegie-Mellon Univ., 1975 (unpublished); R. M. Edelstein *et al.*, Phys. Rev. Lett. 38, 185 (1977).
[16]W. Beusch *et al.*, Phys. Lett. 55B, 97 (1975).